# Trembling Shear Behavior of a Modified-Chitosan Dispersed Suspension under an Electric Field and its Model Study

Young Gun Ko, Ung Su Choi,* Yong Jin Chun

An electro-rheological (ER) fluid showing trembling shear behavior was fabricated with chitosan particles that had benzene, amine and azo-pendent side groups. This modified-chitosan dispersed suspension showed four regions in a plot of shear stress against shear rate at high electric field. We analyzed this specific behavior with our suggested model. The model was developed with the spring-damper model. Our suggested model equation treated the wide range of shear rate and specific behaviors of shear stress in ER fluids. In this study, we successfully obtained various ER fluids showing different behaviors just by changing the side functional groups of the particles in the ER fluids. All of the curves of the shear stress plotted against shear rate were fitted well by our spring-damper model.
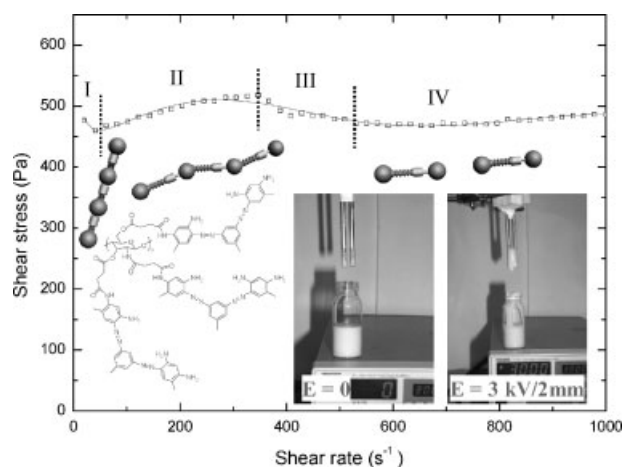
Introduction

Electro-rheological (ER) fluids are a kind of colloidal suspension which rheological properties that can reversibly change over several orders of magnitude under a sufficiently-strong electric field due to the fact that electric field induces interactions between particles, arising from either their dielectric or the conductivity response.[1] Positive ER materials have rheological properties that

Y. G. Ko
Department of Biologic and Materials Sciences, University of Michigan, 1011 North University Ave., Ann Arbor, MI 48109-1078, USA
U. S. Choi
Tribology Research Center, Korea Institute of Science and Technology, P.O. Box 131, Cheongryang, Seoul 130-650, Korea.
Fax: +82-2-958-5659; E-mail: uschoi@kist.re.kr
Y. J. Chun
Department of Cosmetic Science, Chungwoon University, San 29, Namjang, Hongsung, Chungnam 350-701, Korea

dramatically increase with the applied electric field.[2] The specific increase in viscosity of an ER fluid originates from reorientation of dispersed particles whose initially-random distribution transforms into a fibrillated or layered structure, giving rise to a higher viscosity.[3] These properties of ER fluids have stimulated considerable industrial and applied interest.[4] Mundane applications of ER fluids might be in the automobile industry, in which ER-fluid-based shock absorbers would allow the development of fully-active suspensions. Another possible application would be in the suspensions of high-speed magnetically-levitated trains, which would need operating fluids whose response could be modulated quite quickly.[5]

Due to the various potential applications, ER fluids have been studied experimentally[6] and theoretically.[7] Many efforts have been spent on developing high-performance positive-ER materials,[8,9] and many shortcomings are pertinent to these systems, for example, a narrow working temperature, solidification at low temperature, a high

current density due to the high conductivity of water, and device erosion caused by water.[10] Water-free ER fluids have been developed[11] under the assumption that they do not have the shortcomings of hydrous ER fluids. However, anhydrous ER fluids have a different problem - particle sedimentation, which could make ER fluids malfunction and severely limit practical applications.[12] Recently, we synthesized modified chitosans[13] and hollow polyaniline spheres[14] for solving the problem-particle sedimentation as ER materials.

Generally, ER flow shows pseudo-Bingham flow with and without an initial decrease region of the shear stress. In this study, we modified the amine and hydroxy groups of chitosan with various functional groups to observe different ER behaviors. In particular, suspensions dispersed with chitosan coupled with Bismarck brown R showed a trembling behavior of the shear stress with an increase of the electric field. The general theory of the ER effect is the interfacial polarizability of ER particles under an electric field. The interfacial polarizability of ER particles can be enhanced by intercalation, doping, coating, etc. In this study, we got different ER behaviors with the same ER particle material (in this case, chitosan) just by changing the functional groups on the surface of the ER particles.

For the application of ER materials to the industrial field, many models have been developed such as yield stress - electric field,[15] shear stress - dielectric constant,[16] viscosity - shear rate,[17] shear stress - shear rate,[18] for example. The Bingham equation has been used widely as a simple and suitable model for ER fluids.[19] However, complex fluids cannot be explained by that model. Therefore, a model equation using the spring-damper theory of particle-level was suggested in this study. Our suggested model equation treated the wide range of shear rates and specific behaviors of the shear stress in ER fluids.

Experimental Part

Synthesis of Carboxylated and Aminated Chitosans

Chitosan succinate was obtained by the reaction of chitosan (10 g, Jakwang Co., Korea) with succinic anhydride (80 g) in a dimethyl sulfoxide (DMSO) (400 ml, Aldrich Co.) and pyridine (200 ml, Aldrich Co.) solution at 60 °C in an oil bath for 5 h with stirring. After reaction, the modified chitosan was washed with DMSO and distilled, deionized water and dried at 40 °C in a vacuum oven.

Aminated chitosans were synthesized by the following method: chitosan succinate (10 g), triethylamine (50 ml, Aldrich Co.), amine chemicals (0.5 M, Aldrich Co.) and dimethyl sulfoxide (500 ml) were put into a round flask under N_2 purging and reacted at 80 °C in an oil bath for 24 h with stirring. After thereaction, the aminated chitosans were washed with DMSO and distilled, deionized water and dried at 40 °C in a vacuum oven. The amine chemicals were diethylenetriamine, and Bismarck brown R. The aminated chitosans were named as aminated chitosan (I), and aminated chitosan (II), respectively. The substitution yields of chitosan succinate, and aminated chitosan (I), and (II) were 67.5, 92.8, and 36.7%, respectively.

Particle Characterization

The synthesized polymers were ground to 5–30 μm particles using a ball mill. The particles of chitosan, chitosan succinate and aminated chitosans were blended with KBr and then pressed into a disk for analysis. Fourier transform infrared (FT-IR) spectroscopy (GX FT-IR, Perkin Elmer) was used to analyze these particles under nitrogen gas purging. The morphology studies of ER particles were observed using a field-emission scanning-electron micro-scopy (FE-SEM, Hitachi S4200) instrument operating at 15 kV. The sample was mounted on a double-sided adhesive carbon disk and sputter-coated with a thin layer of gold to prevent sample-charging problems. The particle-size distribution was examined by dynamic light scattering (DLS, BI9000AT, Brook Heaven Co. Ltd.).

Suspension Preparation and Electro-Rheological Measurements

The ER fluids were prepared by dispersing the chitosan-derivative particles into silicone oil, whose viscosity was 30 $mm^2 \cdot s^{-1}$ at 25 °C. The silicone oil was dried using molecular sieves before use, and the particle concentration was fixed at 30 vol.-%. The rheological properties of the suspension were investigated in a static DC field using a Physica Couette-type rheometer (Physica US200) with a high-voltage generator. The measuring unit was of a concentric cylindrical type, with a 1 mm gap between the bob and the cup. The shear stress for the suspensions was measured under a shear rate of between 1 and 1 000 s^{-1} and electric fields of 0–3 $kV \cdot mm^{-1}$.

The DC current density J of the chitosan-compounds suspensions were determined at room temperature by measuring the current passing through the fluid upon application of the electric field E_0 and dividing the current by the area of the electrodes in contact with the fluid. The current was determined from the voltage drop across a 1 MΩ resistor in series with the metal cell containing the oil, using a voltmeter with a sensitivity of 0.01 mV. The DC conductivity was taken to be ($\sigma = J/E_0$).

The experimental cell was assembled by mounting two parallel electrodes with a 1 mm gap on a Teflon slide, in which a drop of well-mixed ER fluid was dispersed. The behavior of the ER fluids was observed under 3kV · mm^{-1} using an optical microscope.

Results and Discussion

Fabrication of Anhydrous ER Suspensions and their Electro-Rheological Properties

Chitosan succinate and aminated chitosans were successfully synthesized from chitosan. Figure 1 shows the FT-IR spectra of chitosan, chitosan succinate, aminated chitosan (I), and aminated chitosan (II). After the substitution of the amine and hydroxyl groups with diethylenetriamine, new peaks of C=O (amide group, 1658 cm^{-1}), NH (amide group, 1563 cm^{-1}), C=O (carboxylic group, 1717 cm^{-1}), and C=O (ester group, 1733 cm^{-1}) appeared, as shown in Figure 1(b). After coupling of diethylenetriamine, and Bismarck brown R on chitosan succinate, the peaks of C=O (amide group, 1658 cm^{-1}) and NH (amide group, 1563 cm^{-1}) increased, as shown in Figure 1(c) and (d). The peaks of C=O (carboxylic group, 1717 cm^{-1}) decreased dramatically. The NH$_2$ peak also increased at 1578 cm^{-1}. The N=N peak appeared strongly at 1401 cm^{-1} in Figure 1(d). The chemical structures of the modified chitosans are shown in Figure 1.
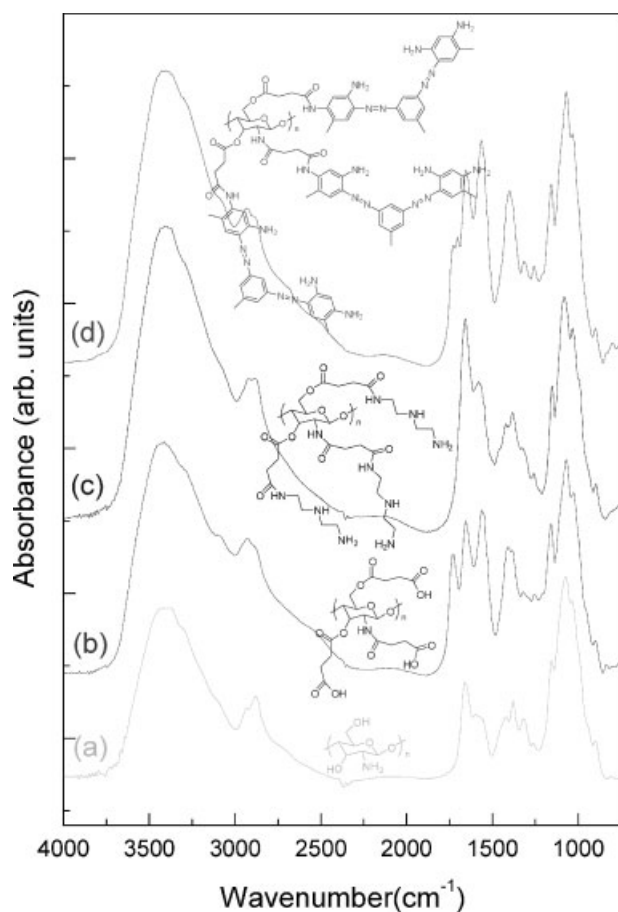

Figure 1. FT-IR spectra of (a) chitosan, (b) chitosan succinate, (c) aminated chitosan (I), and (d) aminated chitosan (II). The chemical structure of each ER material is shown.

The particle shape and size are important for comparison of the ER properties between the different chemical structures of the ER materials. FE-SEM images of used ER particles are shown in Figure 2(a)–2(c). All of the particle shapes are similar and irregular. Figure 2(d) shows the particle-size distribution of the modified chitosans; the average particle sizes of the ER particles are ca. 20 μm (diameter).

Figure 3(a)–3(c) shows the electro-rheological property of an ER fluid visually. In the vial, 30 vol.-% of chitosan succinate was dispersed in silicone oil. The gap between the two rods was 2 mm. The two rods were connected with a high-voltage generator. At 0 kV · mm^{-1}, there was no suspension bridge between the two rods as shown in Figure 3(a). After applying 1.5 kV · mm^{-1}, there was a suspension bridge between two rods as shown in Figure 3(b). This means that the ER strength was stronger than the gravity force acting on the ER fluid. After eliminating the electric field, the bridge of the ER suspension between the two rods was broken, as shown in Figure 3(c). Figure 3(d) and (e) were observed using an optical microscope with 5 vol.-% of chitosan succinate suspension. In Figure 3(d), the electric field is zero; therefore, the particles have a random distribution. In Figure 3(e), an electric field of 3 kV · mm^{-1} has been applied. The presence of fibrils is obvious, although they are not always linear and even have double loops in some cases. These partial fibrils are though to contribute to the viscosity increase, since an attempt to move one electrode relative to the other would be hindered by the drag of the dangling fibrils.

Figure 4(a) shows the conductivity and the current density of the modified chitosan suspensions under various electric fields. The current density and the conductivity of chitosan raw material were very low. Chitosan succinate showed a higher value than chitosan. Only the diethylenetriamine-coupled chitosan suspension showed a very high value. After Bismarck brown R coupling onto the chitosan, the current density and conductivity values were rather higher than those of the chitosan. The electronic properties of most organics are dominated by the weak coupling of the van der Waals-bound molecules. In benzene-ring molecules, the intermolecular coupling is supposed to be stronger because of the significant overlapping between the π electrons clouds supporting the charge-carrier generation and transport leading to a significant delocalization of electrons and, as a consequence, a relatively-significant intrinsic conductivity.[20,21] However, a low current density and conductivity were observed in aminated chitosan (II). In our previous study, chitosan phthalate showed a high current density. If the benzene-ring effect is considered, the results of Figure 4(a) are contrary to previous results. However, this is not surprising if the carboxy and amine groups are
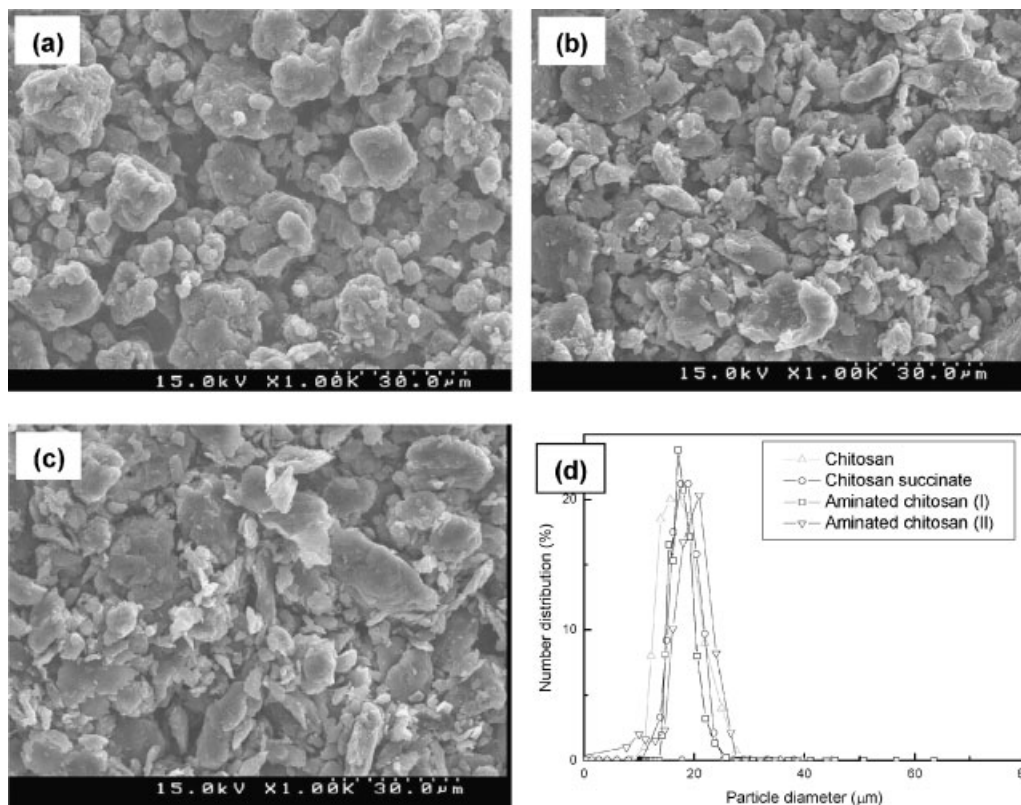
Figure 2. FE-SEM images of (a) chitosan particle, (b) chitosan succinate particle, and (c) aminated chitosan (II) particle. (d) The size distribution of the chemically-modified chitosans. The average particle sizes of the synthesized ER particles are ca. 20 μm (diameter).

considered together. The better π-orbital overlap resulting from the fastening of the benzene rings produces drastic changes of conductivity.[22] There is π-π stacking in chitosan phthalate suspensions under an electric field. However, there is not π-π stacking, but a cation-π interaction under an electric field in the case of aminated chitosan (II). Therefore, the current density and conductivity of aminated chitosan (II) decreased.

Shear stress curves as a function of shear rate for aminated chitosans (II) under 0–3 kV · mm^{-1} electric field are shown in Figure 4(b). This ER material shows a good ER property; however, it does not show typical Bingham plastic behavior. The lines in Figure 4(b) are fitted lines by the Bingham equation. These lines show a large deviation at the high electric field. At high electric field, the curve of the shear stress shows a trembling behavior. To enhance the ER effect, intercalation, doping and coating techniques are used to induce the local-area polarization on the surface of the ER particles. Generally, this modified ER-particle suspension shows pseudo-Bingham behavior under a DC electric field. In the case of the dispersed ER fluid of chitosan particles coupled to Bismarck brown R, trembling behavior was observed with Bingham behavior at a high DC electric field. Therefore, we can consider the

interaction between the side groups on the ER particles under the electric field, although polarization of the ER particles shows predominance. Polarization of particles induces Bingham behavior showing main-flow behavior, and interaction between the side functional groups on the particles induces a stronger bonding increasing ER effect. However, the bonding between the ER particles formed by the interaction between the side functional chains is weaker than the bonding between the ER particles formed by the polarization of the ER particles; therefore it is easy breakable. Therefore, we think carefully that the trembling shear curve was observed due to this bonding. This side-chain effect was also reported in the field of liquid-crystalline (LC) polymers. Jamieson et al showed transient shear-flow behavior on changing the side chains of LC polymers.[23]

Model Schematics Considering the Trembling Behavior of the Shear Stress Plotted against the Shear Rate and its Fitting

The Bingham equation has been used widely as a simple and suitable model for ER fluids with two parameters
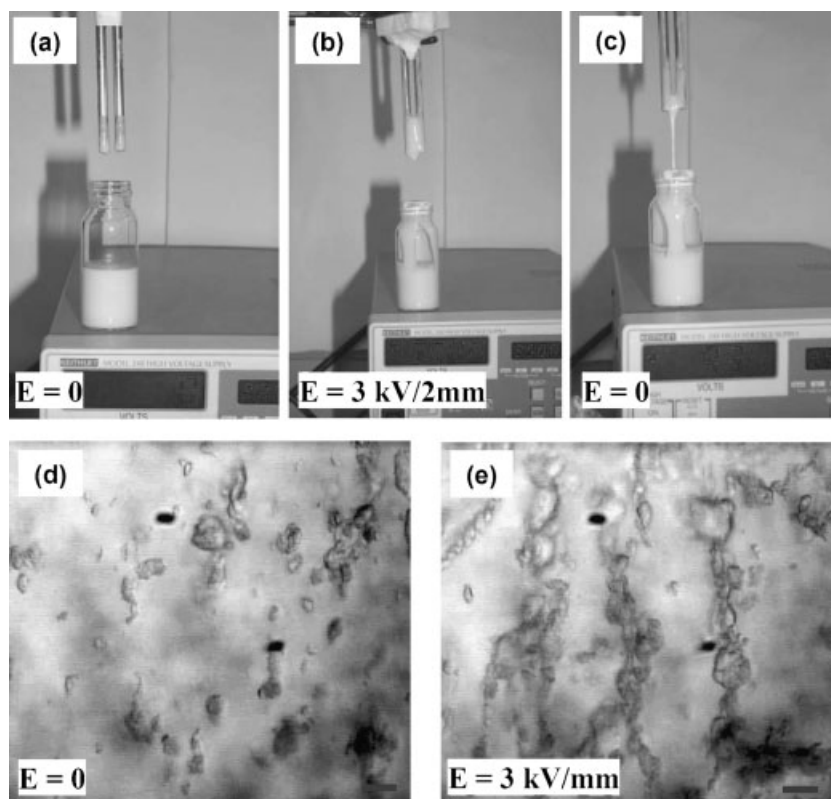
Figure 3. Observation of the ER-fluid behavior between two stainless-steel rods under a $3 \, kV \cdot (2 \, mm)^{-1}$ DC electric field (a) before application, (b) after application, and (c) after elimination of the DC electric field. Optical microscopy images of (d) chitosan succinate suspension and (e) the same portion of the gel after application of a $3 \, kV \cdot mm^{-1}$ DC electric field. The scale of the red bars is 20 μm.

originating from yield stress (τ_0) and Newtonian viscosity η as described below:

$$\tau = \tau_0 + \eta \dot{\gamma} \tag{1}$$

In the phenomena of ER fluids, only pre-yield behavior and Newtonian flow behavior can be explained by this equation. Therefore, this model is not sufficient to describe the plateau regime of the shear stress, which is caused by competition between electrostatic interactions within the particles and hydrodynamic shear flow. To compensate for this, Goodwin et al.[24] and Choi et al.[25] suggested models:

$$\tau = \tau_0 + \dot{\gamma}\eta_0 \left(1 - \frac{\varphi}{\varphi_m}\right)^{-[\eta]\varphi_m} \text{(Goodwin model)} \tag{2}$$

$$\tau = \frac{\tau_0}{1 + (t_2\dot{\gamma})^\alpha} + \eta_\infty \left(1 + \frac{1}{(t_3\dot{\gamma})^\beta}\right)\dot{\gamma} \text{ (Choi model)} \tag{3}$$

Here, τ_0 is the dynamic yield stress, η_0 is the viscosity of the solvent, φ is the packing value, φ_m is the maximum packing value, $[\eta]$ is the intrinsic viscosity, α is related to the decrease in the shear stress, t_2 and t_3 are time

constants, and η_∞ is the viscosity at a high shear rate. The exponent β has the range $0 < \beta \le 1$, since $\frac{d\tau}{d\dot{\gamma}} \ge 0$.

These models can treat the shear stress in the low-shear-rate region well. However, some cases of ER fluids show more-complex curves of the shear stress.[26] The Goodwin model and the Choi model did not treat these complex fluids well. In this study, a new model equation for complex ER fluids is presented.

ER particles are aligned under the electric field, and fibrillar shapes of the aligned ER particles flow along the fluids by shear stress. The structural patterns of the particles suspended in the ER fluids under the electric field are depicted in Figure 5. With the increase of shear rate, the aligned ER particles disassemble from long fibrillar shapes to short fibrillar shapes and particles. During this destruction, there are reforms and distortions between the particles. For our model, we consider that particles are linked to each other by springs and dampers. Even if many models are researched with the concept of springs and dampers for ER fluids,[27] our suggested model, given below, provides more-effective and reasonable fitting than previous models.

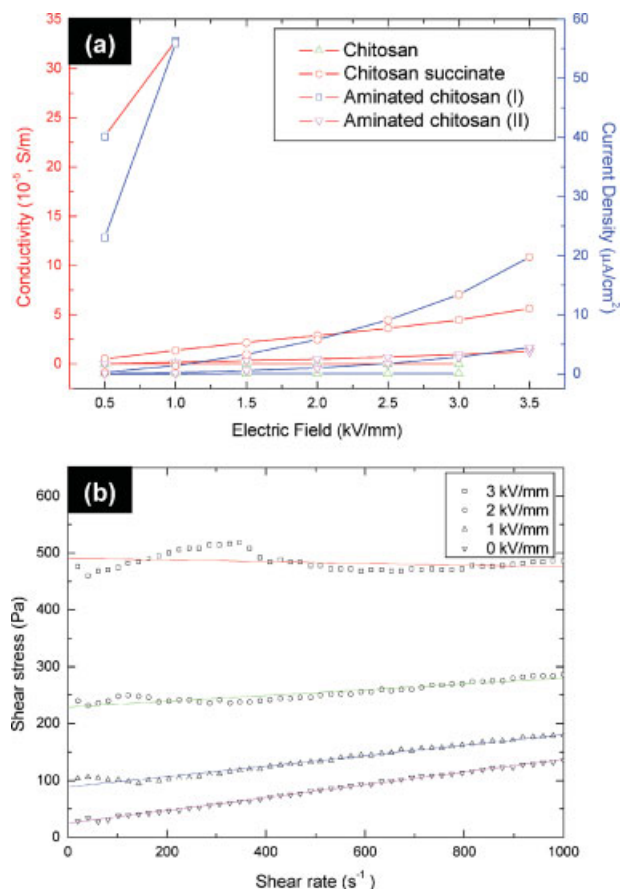$$\tau = \tau_0 + \eta_{app}\dot{\gamma}_{ds} - K_{eff}\gamma_{os} \tag{4}$$

Figure 4. (a) Conductivity (red lines) and current density (blue lines) under various electric field for chitosan (triangles), chitosan succinate (circles), aminated chitosan (I) (squares), and aminated chitosan (II) (inverse triangles), and (b) shear stress vs. shear rate for aminated chitosan (II) under various electric-field strengths. Fits to the plots of shear stress against shear rate are performed using Bingham's equation.

Figure 5. Structural patterns of the particles suspended in the ER fluids under an electric field. The shear rate increases according to the alphabet of figures. The interaction forces between the particles are depicted with springs and dampers. The lengths of the arrows in each figure indicate the speed of the rotated inner bar at the Couette-type rheometer.

Here, τ_0 is the dynamic yield stress, η_{app} is the apparent viscosity, $\dot{\gamma}_{ds}$ is the shear rate of the damping system, K_{eff} is the effective elastic modulus, and γ_{os} is the deformation rate of the oscillation system.

We got an equation from Equation 4 by adjusting the damping and spring model to the ER fluid as shown below:

$$\tau = \tau_0 + \eta_{app}\dot{\gamma}_{ds}$$
$$- K_{eff}e^{-t_1\dot{\gamma}}\{\gamma_1\cos(-t_2\dot{\gamma}) + \gamma_2\sin(-t_2\dot{\gamma})\} \qquad (5)$$

where t_1 and t_2 are time constants, ≥ 0, and γ_1 and γ_2 are deformation-rate coefficients, ≥ 0.

Hao et al. suggested that four kinds of polarization exist in a heterogeneous system: electronic, atomic, Debye, and interfacial polarizations.[28] The Debye and the interfacial polarizations are rather-slow processes, as compared with the electronic and the atomic polarizations. Usually, the former two polarizations are called the slow polarizations,
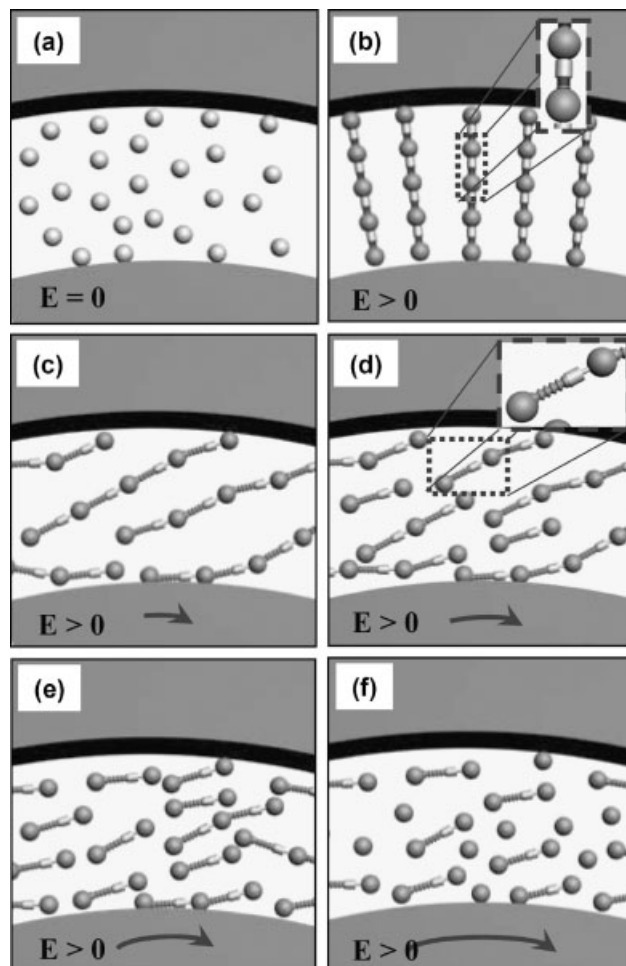
whereas the latter two are the fast polarizations. Huang et al. got lamellar structures after chain structures of ER particles under the electric field from computer simulations, and this agrees very well with their experimental observations.[29] However, it takes time to change from chain structures to lamellar structures. Therefore, we introduce the slipped shear rate $\dot{\gamma}_{slip}$ (≥ 0) in the shear rate of the damping system to compensate for this time gap due to the slow polarization and fully-formed lamellar patterns.

We got Equation 6 by adjusting $\dot{\gamma}_{slip}$ to Equation 5 as shown below:

$$\tau = \tau_0 + \eta_{app}\frac{(\dot{\gamma}-\dot{\gamma}_{slip})^2}{\dot{\gamma}}$$
$$- K_{eff}e^{-t_1\dot{\gamma}}\{\gamma_1\cos(-t_2\dot{\gamma}) + \gamma_2\sin(-t_2\dot{\gamma})\} \qquad (6)$$
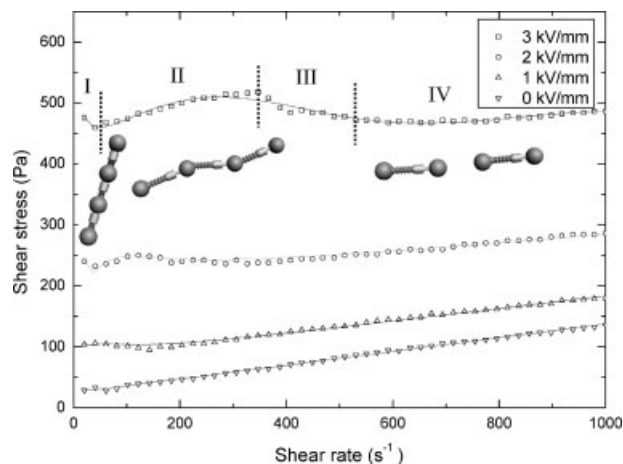
Figure 6. Fit of the suggested model to flow curves for ER fluids based on chitosan coupled to Bismarck brown R with different electric fields. The particle concentration in each of the ER fluids is 30 vol.-%. The insets show structural patterns at that shear rate. In comparison with Figure 4(b), the best fits of shear stress against shear rate are obtained by means of the developed model.

Figure 6 shows an example of a complex ER fluid at high electric field. As the electric field increases, the curves of the shear stress against shear rate become more trembling. Four regions in the curve at 3 kV·mm^{-1} can be distinguished. The behavior showing the decrease of shear stress in region I is due to the slow polarizations and fully-formed lamellar patterns. Even if the immediate effect of the electric field is shown, chain structures of the particles are not fully developed. During the time in which the particles fully-develop, the shear stress decreases for a while. This region is observed only at high electric fields and depends on the chemical structure of the ER particles, and on the electric field.[30] Region II shows a typical ER curve of shear stress against shear rate. In this region, a small amount of fully-developed chain and lamellar structures break by the shear rate because the shear rate is not high. Region III shows an abrupt decrease of the shear stress due to the destruction of the chain and lamellar structures. The lamellar structures are strong but

stiff; therefore, this structure is broken without the slip and the restructure between particles after the endurance of high shear rate. This phenomenon induces a sudden decrease of the shear stress. The exceeding rate of particles-chains destruction is compared to the rate of particles-chains formation. In our experiment, this phenomenon is at one time within the observed region of shear rate. However, in the case of several ER researches, several times of abrupt decrease of the shear stress have been observed.[31,32] This region depends on the chemical structure and particle shapes of the ER particles and on the electric field. In region IV, the destruction rate of the chain and lamellar structures is slow due to the competition of reformation and destruction between the particles. Finally, at a very high shear rate, the value of the shear stress with electric field can be the same as the value without an electric field.[33,34]

According to Equation 6, the experimental data of the shear stress was plotted against shear rate. In comparison with Figure 4(b), the best fits of the shear-stress data against the shear rate are obtained by means of the model developed in this study. The suggested model treated region I to region IV well. The parameters of the suggested model equation are shown in Table 1. Values of τ_0, $\dot{\gamma}_{\text{slip}}$, and t_2 increased with an increase of the electric-field power, and values of η_{app} and t_1 decreased. To confirm the effect on the parameter values, the influence of t_1, t_2, and $\dot{\gamma}_{\text{slip}}$ on the various values are shown in Figure 7(a–c). The t_1, t_2, and $\dot{\gamma}_{\text{slip}}$ parameters were related to the phase intensity, phase difference, and phase delay of the suggested model equation, respectively. In Figure 7(a), t_1 controls the degree of destruction of the aligned ER particles. The degree of destruction of the aligned ER particles decreases with an increase of t_1. We can know that t_1 is related to region III in Figure 6. Increase of t_2 showed the frequency of the aligned ER particles, and the smaller slip effect as shown in Figure 7(b). This parameter was related to the speed and scale of destruction of the aligned ER particles. Figure 7(c) shows the influence of $\dot{\gamma}_{\text{slip}}$ on the curve of shear stress against shear rate. A high $\dot{\gamma}_{\text{slip}}$ describes the high decrease of shear rate in the low shear rate region (region I in Figure 6) well. The curves of shear stress against shear rate

Table 1. Parameters of the suggested model equation, obtained from the curve fitting of ER fluids based on chitosan coupled to Bismarck brown R with different electric fields.

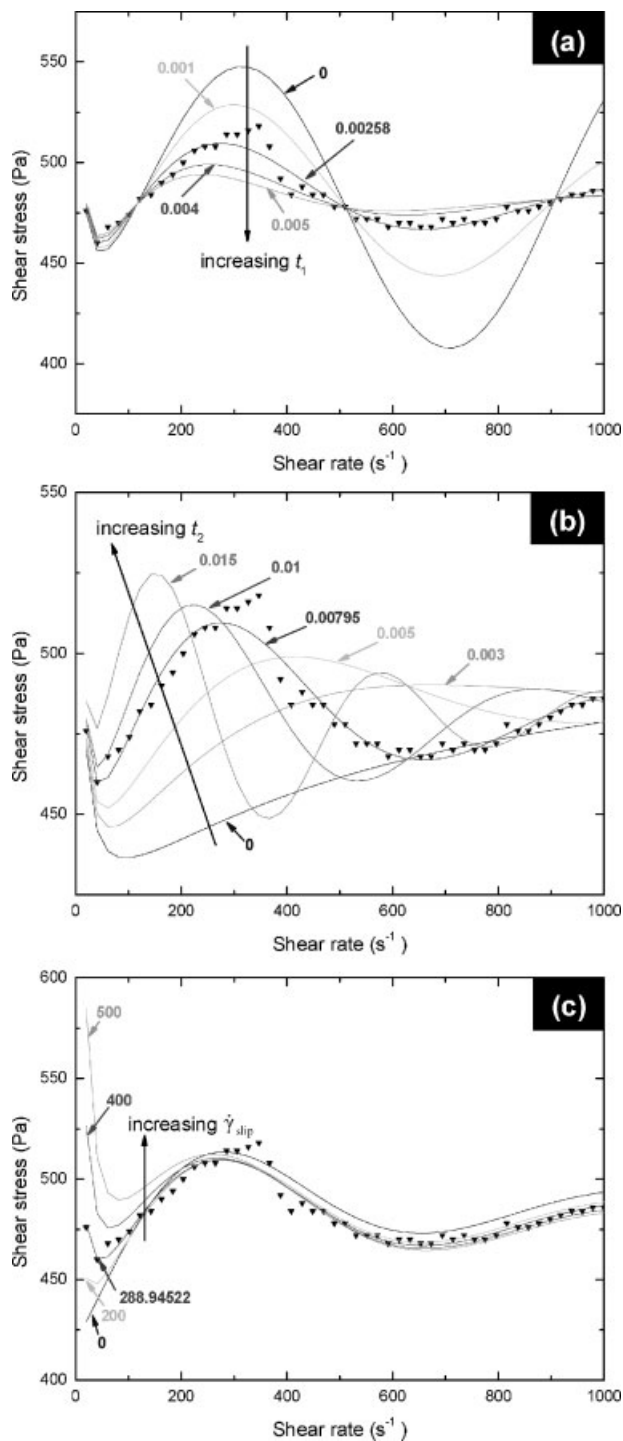| Electric-field strength	τ_0	η_{app}	$\dot{\gamma}_{\text{slip}}$	t_1	t_2	K_{eff}/γ_1	γ_2/γ_1
kV·mm^{-1}	Pa	Pa·s	s^{-1}	s	s	Pa	
0	28.6	0.10679	0	—	—	0	—
1	103.8	0.10610	133.06346	0.05177	0.00001	187.90140	0.60711
2	240.0	0.07792	266.97081	0.03367	0.00020	463.68108	0.65001
3	476.0	0.01382	288.94522	0.00258	0.00795	57.51858	0.74436

Figure 7. The dependence of shear stress on shear rate for different values of (a) t_1, (b) t_2, and (c) $\dot{\gamma}_{slip}$. In these examples, we choose the flow curve of ER fluids based on chitosan coupled to Bismarck brown R at an electric-field strength of $3 \text{ kV} \cdot \text{mm}^{-1}$.

repeats of the destruction of the aligned ER particles, and a decrease of the shear rate in the low shear-rate region cannot be expressed if there are no t_1, t_2, and $\dot{\gamma}_{slip}$ parameters in our suggested model equation. By confirming the influence of the model parameters, we can get the conclusion with Table 1 and Figure 6; at low shear rate, the fast and extensive alignment of the particles in the ER suspension occurs in the high electric field; however, the alignments are unstable and reform again to fully-formed lamellar patterns. After forming lamellar structures of particles in the ER suspension, the destruction degree of the aligned ER particles decreases, and the destruction frequency of the aligned ER particles increases with the increase of electric field. The value of τ_0 of the ER fluid increased with the increase of the electric field as shown in Table 1 and Figure 6. In brief, a high yield stress is obtained at high electric field, however the fibrillar and lamellar structures of the particles in the ER suspension are weak.

We applied Equation 6 to other modified chitosan-based ER fluids as shown in Figure 8. The suggested equation treated all of the curves of shear stress against shear rate well. Although the shapes and size distributions of the modified chitosan particles were the same, they each showed different curves of shear stress against shear rate. In the case of (a) and (b), there are no regions I and III, which were explained in Figure 6. Only Figure 8(c) showed a decrease of the curve as in region III. By this result, we can know that curve shape of the shear stress against shear rate of modified chitosan-based ER fluids can depend on the chemical structure.

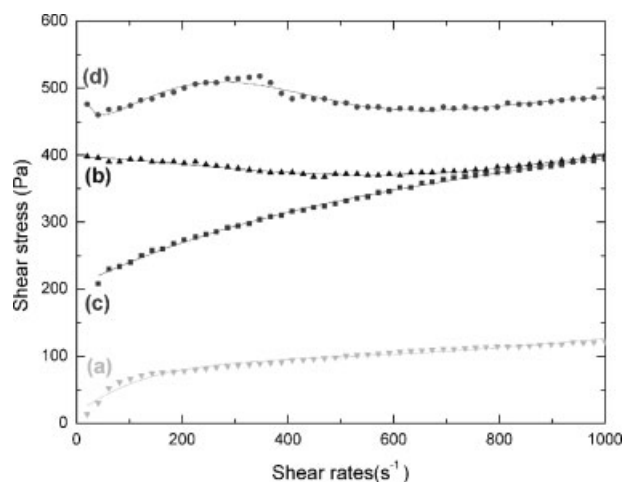The chitosan succinate suspension showed a higher shear stress than chitosan. However, after coupling of

Figure 8. Fit of the suggested model to flow curves for (a) chitosan particles, (b) chitosan succinate particles, (c) aminated chitosan (I), and (d) aminated chitosan (II)-based ER fluids at an electric field strength of $3 \text{ kV} \cdot \text{mm}^{-1}$. The particle concentration of each ER fluid is 30 vol.-%.

can be explained well by the effects of these parameters, in that the increase of $\dot{\gamma}_{slip}$, the decrease of t_1, and the increase of t_2 were shown with the increase of shear rate in Figure 6. In brief, a slow destruction of the aligned ER particles,

diethylenetriamine onto chitosan succinate (named as aminated chitosan (I)), the shear stress decreased. After coupling of Bismarck brown R onto chitosan succinate (named as aminated chitosan (II)), the shear stress increased. This result is different to our previous study.[13] In our previous study, various carboxyl groups were coupled to chitosan. In that study, although expecting intermolecular overlapping between the π electrons, chitosan phthalate showed a lower shear stress than chitosan succinate. However, in this study, aminated chitosan (II), which has a benzene ring, showed a higher shear stress than chitosan succinate. Because the carboxylic group is an anion, there is only the intermolecular overlapping between the π electrons in chitosan phthalate. However, in the case of aminated chitosan (II), there are both an amine group and a benzene ring. Because the amine group is a cation, cation-π interactions can be expected, together with π-π stacking.[35] In particular, the cation-π interaction is stronger than the π-π stacking. Aminated chitosan (II) showed interesting behavior with the decrease of the shear stress in the low shear rate range for higher applied electric fields. In general, the suspended particles rotate around the applied shear field, and the angular velocity is related to the shear rate. Therefore, even under a DC electric field, particles or clusters behave as if they were in an AC electric field during flow. Thus, aminated chitosan (II) cannot be fully polarized during flow, and the structures developed under DC electric fields in the absence of flow cannot be maintained when the deformation starts, so that initially the shear stress decreases with shear rate. By these phenomena, the trembling behavior of shear stress on shear rate can be explained well.

model equation is very useful and meaningful for the curve fitting of the shear stress against shear rate, and gives a good explanation of the experimental data. By fitting the shear-stress curve with our suggested model, we can know that the high yield stress is obtained at high electric field; however, the fibrillar and lamellar structures of the particles in the ER suspension are weak. At the low shear rate, fast and extensive alignment of the particles in the ER suspension occurs in the high electric field; however, the alignments are unstable and reform again to fully-formed lamellar patterns. After forming lamellar structures of the particles in the ER suspension, the destruction degree of the aligned ER particles decreases, and the destruction frequency of the aligned ER particles increases with the increase of the electric field. Modified chitosan-based ER fluids showed various curves of shear stress against shear rate along their chemical structures, and all of the curves were fitted well with our suggested equation. We knew that each of the ER fluids showed different curves of shear stress against shear rate, although the shapes and size distributions of the modified chitosan particles were the same. By this result, we can know that various ER fluids showing different behavior can be obtained just by changing the side functional groups of the particles in the ER fluids. We hope that our suggested model equation of shear stress vs. shear rate, and experimental results help the development of ER materials.

Conclusion

In this study, carboxyl groups and amine groups were coupled to chitosans as novel anhydrous ER materials. Dispersed suspensions of the synthesized ER materials show different behaviors of shear stress against shear rate to each other. In particular, chitosan coupled to Bismarck brown R showed a trembling behavior of the shear stress. We divided this behavior into 4 regions; I) a region for the slow polarizations and fully-formed lamellar patterns, II) a region for an increase of the shear stress with increased shear rate after fully-formed fibrillar and lamellar patterns, III) a region for an abrupt decrease of the shear stress due to the destruction of the chain and lamellar structures, and IV) a region for the slow-destruction rate of the chain and lamellar structures due to the competition of reformation and destruction between the particles. For the analysis of this behavior, we suggested a new model equation with the spring-damper theory. Our suggested

[1] T. C. Halsey, *Adv. Mater.* **1993**, *5*, 711.
[2] I. S. Sim, J. W. Kim, H. J. Choi, C. A. Kim, M. S. Jhon, *Chem. Mater.* **2001**, *13*, 1243.
[3] T. Hao, *Adv. Mater.* **2001**, *13*, 1847.
[4] D. L. Hartsock, R. F. Novak, G. J. Chauny, *J. Rheol.* **1991**, *35*, 1305.
[5] E. Pennisi, *Sci. News* **1992**, *141*, 55.
[6] L. Liu, X. Chen, X. Niu, W. Wen, P. Sheng, *Appl. Phys. Lett.* **2006**, *89*, 083505.
[7] Y. Tian, Y. Meng, S. Wen, *Appl. Phys. Lett.* **2006**, *88*, 094106.
[8] V. Parlínek, P. Sáha, O. Quadrat, J. Stejskal, *Langmuir* **2000**, *16*, 1447.
[9] U. S. Choi, Y. G. Ko, J. Y. Kim, *Polym. J.* **2000**, *32*, 501.
[10] A. Inoue, Y. Ide, H. Oda, *J. Appl. Polym. Sci.* **1997**, *64*, 1319.
[11] X. P. Zhao, J. B. Yin, *Chem. Mater.* **2002**, *14*, 2258.
[12] L. Xiang, X. Zhao, *J. Colloid Interface Sci.* **2006**, *296*, 131.
[13] Y. G. Ko, U. S. Choi, *J. Appl. Polym. Sci.* **2006**, *102*, 4937.
[14] B. H. Sung, Y. G. Ko, U. S. Choi, *Colloids Surf. A* **2007**, *292*, 217.
[15] H. J. Choi, M. S. Cho, J. W. Kim, C. A. Kim, M. S. Jhon, *Appl. Phys. Lett.* **2001**, *78*, 3806.
[16] Y. Lan, S. Men, X. Zhao, K. Lu, *Appl. Phys. Lett.* **1998**, *72*, 653.

[17] K.-L. Tse, A. D. Shine, *Macromolecules* **2000**, *33*, 3134.

[18] Y. D. Kim, D. D. Kee, *AIChE J.* **2006**, *52*, 2350.

[19] D. J. Klingenberg, C. F. Zukoski, IV *Langmuir* **1990**, *6*, 15.

[20] M. Knupfer, T. Schwieger, J. Fink, K. Leo, M. Hoffmann, *Phys. Rev. B: Condens. Matter Mater Phys.* **2002**, *66*, 352081.

[21] A. Stanculescu, F. Stanculescu, H. Alexandru, M. Socol, *Thin Solid Films* **2006**, *389*, 393.

[22] J. Roncali, *Chem. Rev.* **1997**, *97*, 173.

[23] N. Yao, A. Jamieson, *Macromolecules* **1998**, *31*, 5399.

[24] J. W. Goodwin, G. M. Markham, B. Vincet, *J. Phys. Chem. B* **1997**, *101*, 1961.

[25] M. S. Cho, H. J. Choi, M. S. Jhon, *Polymer* **2005**, *46*, 11484.

[26] H. J. Choi, J. H. Lee, M. S. Cho, M. S. Jhon, *Polym. Eng. Sci.* **1999**, *39*, 493.

[27] T. Butz, O. von Stryk, *Z. Angew. Math. Mech.* **2002**, *82*, 3.

[28] T. Hao, A. Kawai, F. Ikazaki, *Langmuir* **1998**, *14*, 1256.

[29] J. G. Cao, J. P. Huang, L. W. Zhou, *J. Phys. Chem. B* **2006**, *110*, 11635.

[30] F. F. Fang, J. H. Kim, H. J. Choi, *Macromol. Symp.* **2006**, *242*, 49.

[31] Y. G. Ko, U. S. Choi, B. H. Sung, *J. Appl. Polym. Sci.* **2004**, *93*, 1559.

[32] M. Ciszewska, A. Krztoń-Maziopa, J. Płocharski, *Polym. Adv. Technol.* **2006**, *17*, 41.

[33] M. S. Cho, Y. H. Cho, H. J. Choi, M. S. Jhon, *Langmuir* **2003**, *19*, 5875.

[34] J.-B. Jun, S.-Y. Uhm, K.-D. Suh, *Macromol. Chem. Phys.* **2003**, *204*, 451.

[35] J. W. Steed, J. L. Atwood, ''*Supramolecular Chemistry*'', John Wiley & Sons, Chichester, UK 2000.